Draft version July 8, 2014
Preprint typeset using LaTeX style emulateapj v. 5/2/11

SPATIALLY RESOLVED HCN J=4–3 AND CS J=7–6 EMISSION FROM THE DISK AROUND HD 142527

G. van der Plas[1,2], S. Casassus[1,2], F. Ménard[2,3,4], S. Perez[1,2], W. F. Thi[3], C. Pinte[3,4] and V. Christiaens[1,2]
Departamento de Astronomia, Universidad de Chile, Casilla 36-D, Santiago, Chile
Millenium Nucleus Protoplanetary Disks in ALMA Early Science, Universidad de Chile, Casilla 36-D, Santiago, Chile
Univ. Grenoble Alpes, IPAG, F-38000 Grenoble, France CNRS, IPAG, F-38000 Grenoble, France and
UMI FCA, CNRS / INSU France, and Dept. de Astronomia y Obs. Astronomico Nacional, Universidad de Chile, Casilla 36-D, Correo Central, Santiago, Chile (UMI 3386)

Draft version July 8, 2014

ABSTRACT

The disk around HD 142527 attracts a lot of attention, amongst others because of its resolved (sub) mm dust continuum that is concentrated into a horseshoe-shape towards the north of the star. In this manuscript we present spatially resolved ALMA detections of the HCN J=4–3 and CS J=7–6 emission lines. These lines give us a view deeper into the disk compared to the (optically thicker) CO isotopes. This is the first detection of CS J=7–6 coming from a protoplanetary disk. Both emission lines are azimuthally asymmetric and are suppressed under the horseshoe-shaped continuum emission peak. A possible mechanism to explain the decrease under the horseshoe-shaped continuum is the increased opacity coming from the higher dust concentration at the continuum peak. Lower dust and/or gas temperatures and an optically thick radio-continuum reduce line emission by freeze-out and shielding of emission from the far side of the disk.

Subject headings: circumstellar matter, stars: pre-main-sequence, protoplanetary disks, stars: individual (HD 142527)

1. INTRODUCTION

High resolution spatially resolved observations of protoplanetary disks with a gap or central hole, i.e., transitional disks, show that these disks often are rich in azimuthal structure. These asymmetries can be divided in two groups that either trace the disk surface or the disk mid plane. Scattered light (e.g. Fukagawa et al. 2006) and ^{12}CO molecular line observations, e.g. spiral arms (Christiaens et al. 2014), trace the disk surface. Radio continuum observations trace the bulk of the dust mass in the disk mid plane. Asymmetries in the latter are interpreted as a clustering of larger (mm sized) dust particles (e.g. LkHa 330, SR 21 and HD 135344B (Brown et al. 2009; Pérez et al. 2014), HD 142527 (Casassus et al. 2013) and IRS 48 (van der Marel et al. 2013)) and can be explained by the presence of local pressure maxima which 'trap' the dust (see e.g. Lyra & Lin 2013, and references therein for an overview). In theory, these dust traps would correspond to local minima of the gas-to-dust ratio. Such an atypical physical environment represents an interesting laboratory for gas chemistry.

The disk with the best studied dust trap can be found currently around HD 142527, a nearby (145 pc, Acke & van den Ancker 2004) Herbig Ae/Be star of spectral type F6III. This star is surrounded by a large disk with an inclination estimated to be between $\approx 20°$ (Verhoeff et al. 2011) and $28\pm5°$ (Perez et al. submitted) and a Position Angle (PA) of 160°. For the analysis presented in this manuscript we adopt the latter value of the disk inclination. A large opacity gap seen in continuum emission both in scattered light and (sub-) mm emission separates the inner ($\approx$ 10 au, van Boekel et al. 2004) and outer disk (≈140 au, Fukagawa et al. 2006). The outer disk is rich in spiral structure when imaged in scattered light (Fukagawa et al. 2006; Casassus et al. 2012; Rameau et al. 2012; Canovas et al. 2013; Avenhaus et al. 2014) and, at larger scales, CO rotational lines (Christiaens et al. 2014). Using ALMA at 870 μm, the outer disk is resolved into a horseshoe-shaped dust continuum that peaks at a PA of 35° at radial distance of $\approx 1''$ (Casassus et al. 2013; Fukagawa et al. 2013) with a surface intensity contrast ratio of $\approx$ 30 compared to the minimum of the continuum emission at similar radius on the other side of the star. Various J=3-2 and J=2-1 CO isotopes have been detected coming from the outer disk but also from within the gap, and HCO+ J=4–3 emission is seen from the outer disk with a decrement coincident with the horseshoe-shaped dust continuum and in two gap-crossing filaments (Casassus et al. 2013).

In this manuscript we present the detection of the HCN J=4–3 and CS J=7–6 emission lines at rest frequencies of respectively 354.50547 and 342.88286 GHz from the disk around HD 142527. HCN is a molecule commonly detected from disks (e.g. Dutrey et al. 1997; Thi et al. 2004; Kastner et al. 2008; Fuente et al. 2010; Öberg et al. 2010, 2011). The J=4–3 transition has a critical density n_{crit} of 8.5 $\times 10^6$ cm^{-3} (Thi et al. 2004). Its dominant destruction mechanisms in disks are accretion onto dust grains, charge transfer reactions with H^+, the ion-molecule reaction with C^+, protonation reactions with H_3^+, HCO^+, and $H3O^+$ and, higher up in the disk at $\approx$ 1.5 - 2 scale heights, photodissociation by stellar UV photons (Semenov & Wiebe 2011).

CS emission has been detected coming from a few disks (e.g. CS J=5–4 and J=3–2, Dutrey et al. 1997; Fuente et al. 2010; Guilloteau et al. 2012). The J = 7–6 line presented in this work is the first time that this rotational transition is detected from a disk. CS is a gas phase reservoir for sulfur and especially its higher rotational transitions appear to be good tracers for dense gas because of their relatively high critical densities (n_{crit} = 2.9 $\times 10^6$ cm^{-3} for J=7–6, Thi et al. 2004). CS destruction pathways are photodissociation in the disk atmosphere, depletion onto dust grains, slow endothermic oxidation reaction (CS + O → CO + S), charge transfer with ionized hydrogen atoms, and ion-molecule reactions with primal ions, e.g. HCO^+ , H_3O^+ , and H_3^+ (Semenov & Wiebe 2011).

2. OBSERVATIONS AND DATA REDUCTION

For the observing strategy and data reduction we refer to Casassus et al. (2013). In short summary: imaging of the CS and HCN lines was performed using the CLEAN task in CASA (Högbom 1974). The data presented in this manuscript are binned in spectral channels of width 0.214 km s^{-1} and CLEANed to a RMS noise level of 12 mJy / channel with a synthesized beam size of $0.56'' \times 0.35''$ and a PA of 67°.

We note that the default continuum subtraction scheme in the visibility domain left residuals which stand out as extended negatives following the horseshoe shape of the continuum in the spectral vicinity of the CS J=7–6 line. We found no continuum subtraction artifacts in the spectral vicinity of the HCN J=4–3 line. We correct for this by sampling an average continuum subtraction artifact from the spectral channels within 7 km s^{-1} on either side of the affected line between respectively -6 and 1 km s^{-1} and 6 and 13 km s^{-1}. We subtract this average from all spectral channels used in our analysis of the CS J=7–6 line. Removing these negatives had the effect of increasing the integrated CS J=7–6 line flux by 38%.

3. RESULTS

We detect HCN J=4–3 and CS J=7–6 emission from the outer disk around HD 142527. We show the CS J=7–6 and HCN J=4–3 integrated intensity, velocity and peak intensity maps in Figure 1, the integrated emission lines in Figure 3 and the azimuthal brightness variation in Figure 4. The segmented appearance of the peak intensity maps is caused by discretization of the velocity field in channel-averaged visibilities, discussed in Christiaens et al. (2014). Both emission lines vary as function of azimuth and are suppressed in regions with strong continuum emission. The HCN J=4–3 line originates from radii smaller than the CS J=7–6 emission at all azimuths. In the outer disk, CS J=7–6 and HCN J=4–3 emission is detected beyond the horseshoe, and HCN J=4–3 marginally on its inside as well. The emission for both lines is strongest close to where the continuum emission is weakest (c.f. Figure 5).

We see no counterpart for the CS and HCN emission with the spiral structure seen in scattered light and CO rotational lines. We discuss the CS and HCN emission in detail in sections 3.1 and 3.2, respectively.

3.1. *CS J=7–6*

The integrated CS J=7–6 line shows a double peaked line profile with a FWHM of 2.71 ± 0.21 km s^{-1} and an integrated flux of 1.67±0.08 Jy km s^{-1} (1 σ ignoring calibration uncertainties). The CS emission traces the outer disk, and there is a strong asymmetry between the near and far side of the disk. In the outer disk the emission is strongest towards the south west (PA = 200° - 240°), while there is only faint emission coming from the region co-spatial to the peak continuum emission. We show the radial intensity cuts in the direction of the peak molecular and peak continuum emission in the right panel of Figure 5.

3.2. *HCN J=4–3*

The integrated HCN J=4–3 line shape is similar to that of the CS line, but only shows the red peak. The line FWHM is 2.52 ± 0.21 km s^{-1} and has an integrated flux of 1.73 ± 0.05 Jy km s^{-1} (1σ ignoring calibration uncertainties). Compared to the CS J=7–6 line, it traces the disk up to about the same outer radius but a smaller inner radius. The radially integrated emission is strongest towards the south west (between 200° and 240°), and is weakest where the continuum emission peaks. Emission inside the disk gap is detected at 4 and 6 σ confidence levels to the east and west of the star respectively in individual channel maps between 3 and 3.4 km s^{-1}, at similar velocities and location as the gap-crossing streams visible in the HCO+ J=4–3 reported in Casassus et al. (2013). The radial intensity cuts in the direction of the peak molecular and peak continuum emission are shown in Figure 5.

We note that Öberg et al. (2011) report a 2σ upper limit of 0.77 Jy km s^{-1}) on the HCN J=3–2 emission line. Assuming that the HCN J=4–3 and J=3–2 emission lines are emitted from the same region, optically thin and in LTE, the HCN J=3–2 2 σ upper limit is consistent with the HCN J=4–3 detection if the excitation temperature is $T_{ex} \geq 30$ K.

4. DISCUSSION

Both the brightness of the eastern side of the disk in thermal mid-IR emission (Fujiwara et al. 2006; Verhoeff et al. 2011) and the trailing spiral arm towards the west (Fukagawa et al. 2006; Casassus et al. 2012; Christiaens et al. 2014) suggest that the far face of the disk is located towards the ENE. This orientation and the fact that the CS emission originates from distances larger than the inner rim (c.f. Figure 5) rule out emission from the inner rim of the outer disk inclined into the line of sight as source for the brightness asymmetry most clearly seen in the CS emission.

In the following discussion, we assume that the horseshoe-shaped continuum emission from the disk around HD 142527 is caused by dust being trapped, e.g. in a vortex, which leads to a locally enhanced dust to gas ratio and a different dust size distribution (Birnstiel et al. 2013). The lack of CS and HCN emission under the horseshoe can be qualitatively understood when considering the implications of these different local dust properties on the presence of gas-phase CS and HCN molecules in the dust trap. The dust provides extra surface for surface-chemistry reactions and modifies the local temperature and radiation field. Additionally, the dust trap may be optically thick even in the sub-mm continuum and have a noticeable effect on the molecular emission line.

4.1. *Temperature and chemistry*

Within the dust trap. A pressure maximum preferentially traps larger grains. This size sorting has the effect of increasing the local average grain size which in turn drives a lower dust temperature because the ratio of the mass opacity κ_ν in the optical and far-IR is lower for larger grains (Miyake & Nakagawa 1993).

The impact of an increased dust-to-gas ratio on gas temperature is not straightforward to quantify. Dust influences the gas temperature both through cooling by thermal accommodation and through heating by photo-electric heating. Increased dust-to-gas ratios better thermalize the gas which can decrease the reservoir of thermally decoupled gas, and also plays a role in the chemistry balance. Higher dust abundances provide increased attenuation of the UV radiation field and thus shielding against photo-dissociation and photo-desorption. An enhanced dust abundance furthermore provides extra surface for chemical processes such as the freeze-out of CO, H_2O, CS and HCN molecules. Modeling the effect of a dust trap on the local gas temperature is beyond the scope of this manuscript. For a discussion on the effect of increasing the dust to gas ratio on the gas temperature see Chapter 6 of

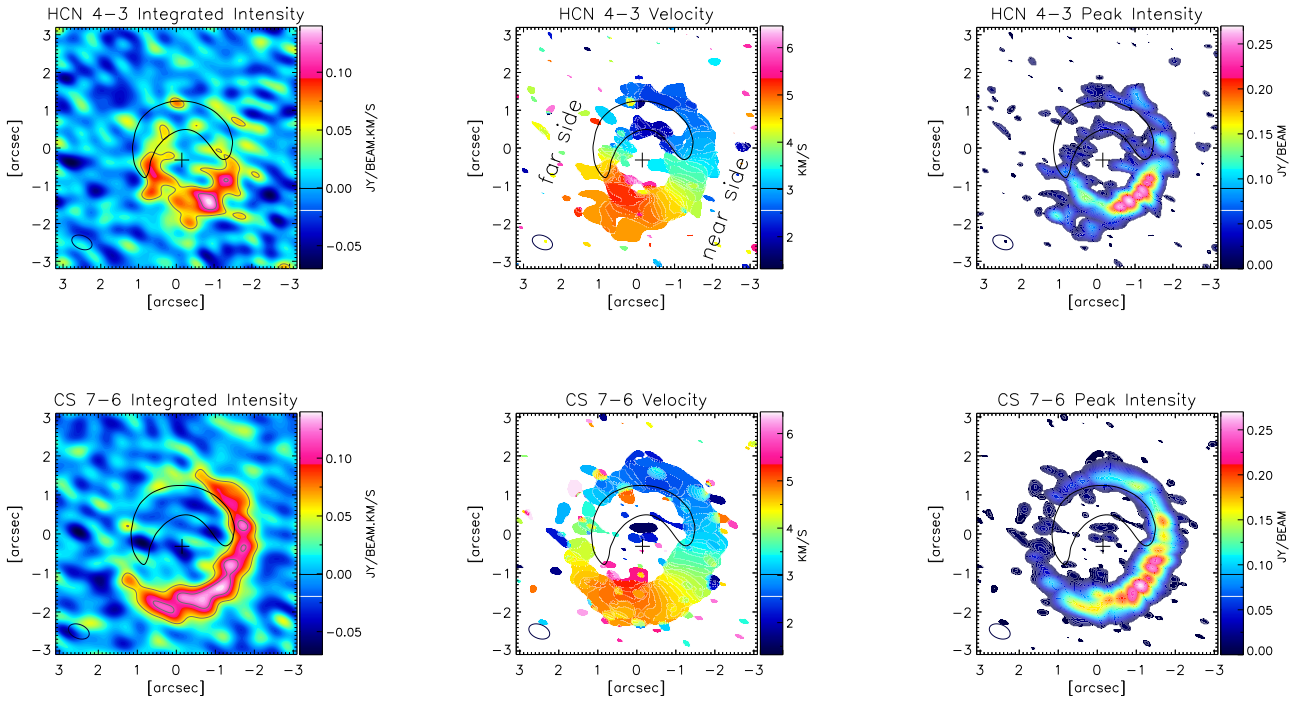

FIG. 1.— CS J=7–6 (top row) and HCN J=4–3 (bottom row) integrated intensity (left), velocity centroid $v_\circ$ (middle) and peak intensity $I_{\rm peak}$ (right). The $v_\circ$ and $I_{\rm peak}$ maps have been created using the maximum intensity of the spectrum at each location providing a $\geq 3\,\sigma$ signal. Overplotted on the integrated intensity map are intensity contours spaced at 3 times the noise level of this map (respectively 0.014 and 0.018 Jy km s^{-1} beam^{-1} for CS J=7–6 and HCN J=4–3). The $v_\circ$ and $I_{\rm peak}$ maps are obtained using all signal above 3 times the RMS as determined from individual channels not containing line emission. The x and y axis are labeled in arcseconds, north is up and east is left. The position of the star is given by a plus sign and the beam is shown in the bottom left. With a black line we show the dust continuum emission at 30% of it's maximum. For clarity we mark the near and far side of the disk in the velocity centroid map of the HCN 4–3 emission.

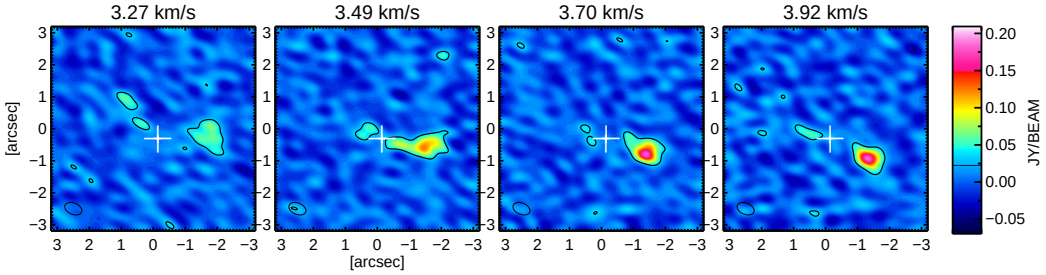

FIG. 2.— Selected channel maps showing 3 channels of the HCN 4–3 emission within the gap near the systemic velocity of 3.6 km s^{-1}. The black contour denotes 0.2 × the peak intensity of the moment 8 map. Notation is similar to that in Figure 1.

van der Plas (2010), who find that increasing the dust to gas mass ratio with a factor of 10 led to a decrease in gas temperature and reduced the amount of thermally decoupled (from the dust, i.e. gas which is possibly contributing to line emission) CO gas by a factor of 3.

Observations that support this interpretations are the local minima observed in the ^{13}CO and C^{18}O J = 2-1 isotopologues co-spatial to the horseshoe shaped dust continuum emission (Perez et al. submitted), which can be interpreted as a lower temperature at the line-forming region or the freeze-out of CO molecules. Abundant crystalline water ice has also been detected from the outer disk (Malfait et al. 1999; Honda et al. 2009). CS and HCN in disks both freeze out at temperatures of ≈ 50 to 60K (Garrod & Herbst 2006), between the condensation temperatures of CO and H_2O. Based on the peak of the SED at 60 μm in the ISO spectrum published by Malfait et al. (1999) we estimate the dust temperature inside the dust trap, which emits the bulk of the (sub-)mm emission, to be ≈21 K.

Outside of the dust trap, lower opacities in the UV lead to a higher sublimation and photodissociation rate and temperature deeper in the disk. CS molecules can form at low scale height in those regions of the disk where water freezes out and CO does not (T between ≈ 20 and 100 K for a typical disk). Water ice traps gas-phase oxygen atoms and prevents the formation of CO, which in turn frees up carbon atoms to form reduced species such as CH and CH_2. These molecules can react with sulfur atoms to form CS. HCN molecules have less stringent formation conditions and can reach detectable concentrations higher up in the disk and closer to the star compared to CS molecules (Walsh et al. 2010).

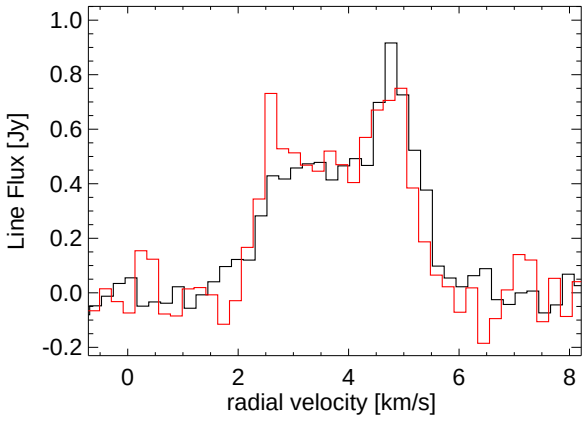

FIG. 3.— HCN J=4–3 (black) and CS J=7–6 (red) emission lines extracted with an elliptical extraction aperture with a semi-major axis of 2.4″ encompassing the disk and a velocity resolution of 0.214 km s^{-1} per bin. The integrated line fluxes are 1.73 ± 0.05 Jy km s^{-1} and 1.67±0.08 Jy km s^{-1}, and the FWHM values 2.52 ± 0.21 km s^{-1} and 2.71 ± 0.21 km s^{-1} respectively for the HCN and CS line.

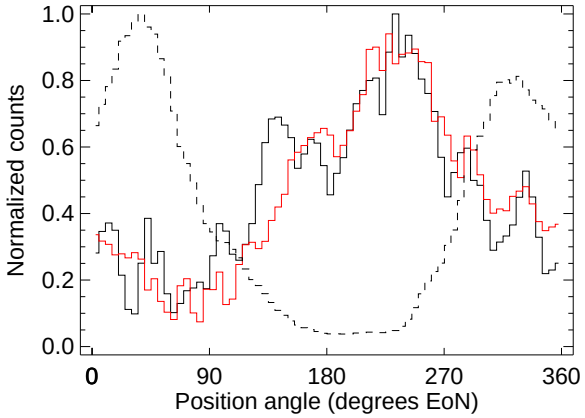

FIG. 4.— Scaled HCN J=4–3 (black) and CS J=7–6 (red) azimuthal intensity profiles extracted from the peak intensity map using a ring projected to match the disk inclination and PA between 0.4″ and 2.2″ (c.f. the two right panels of Figure 1). The scaled continuum intensity is shown with a dashed black line for comparison. See figure 5 for the radial intensity cuts at the peak continuum and line emission.

4.2. *Optically thick continuum*

Continuum opacity effects - a (partially) optically thick outer disk - are an alternative explanation of the attenuated molecular emission under the dust trap. HD 142527 is extremely bright in the sub-mm and to fit the observed (sub-) mm emission a dust mass of 1.0 × 10^{-3} M$_\odot$ is required. This model has a maximum opacity at 850 μm of τ = 2.76 at the inner rim of the outer disk. (private communication, Verhoeff et al. 2011). Given the peak flux of 0.36 Jy/beam and beam size of 0.51″ × 0.33″ (Casassus et al. 2013), the Rayleigh-Jeans equivalent brightness temperature of the peak dust emission is ≈20 K and similar to our estimate of the dust temperature. The band 7 continuum is of similar size of the beam and, if radially unresolved, likely to be optically thick.

To check whether shadowing by such an axisymmetric inclined optically thick ring can produce asymmetric features caused by the interception of molecular line emission from the far side of the disk in the line-of-sight towards the observer such as e.g. the near/far asymmetry as seen in the CS emission maps, we use the radiative transfer model code MCFOST (Pinte et al. 2006, 2009). With a disk model resembling the disk architecture of HD 142527 (the same disk inclination, PA, and mass, consisting of an inner disk, a disk gap and an outer disk) we explore a range of models for which, in the inner rim of the outer disk, we vary the dust mass m$_{dust}$, the CS abundance $\epsilon_{\rm CS}$ and the dust to gas ratio δ. Within a parameter space where we vary m$_{dust}$ in the inner rim (between 5 and 30 au wide) between 6.6e-4 × M$_\odot$ and 4.5e-2 × M$_\odot$, $\epsilon_{\rm CS}$ between 3.5e-9 and 3.5 e-11, and δ between 1 and 100, we fail to reproduce emission maps in which the near side of the inner edge of the outer disk is brighter than the far side.

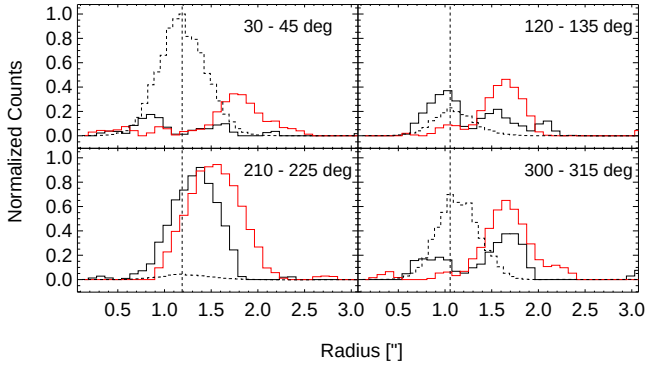

FIG. 5.— Radial intensity profiles of HCN J=4–3 (black), CS J=7–6 (red) and continuum (black, dashed) emission in four directions: One coincident with the peak continuum emission (top left panel, between 30° and 45° EoN), one coincident with the radially integrated peak line emission (bottom left panel, between 210° and 225° EoN), and two intermediate angles. The radial profiles have been extracted from the peak intensity maps and normalized to their respective global maximum in the disk. We mark the radial location of the peak continuum emission for clarity with a vertical striped line.

The concentration of dust particles in a dust trap locally instead of in an axisymmetric ring enhances the local optical depth further, which in turn can be invoked to explain the horseshoe-shaped decrement observed in the HCN and HCO+ J=4-3 and the CO J=2-1 lines.The emission on the far side of the optically thick regions is absorbed, while only excess temperature relative to the cold background leads to emission on the near side. Thus an optically thick horseshoe will impart a similarly shaped decrement in line emission maps seen face-on, with some modulation depending on the vertical temperature structure and on the vertical location of the τ = 1 surface.

5. CONCLUSIONS

We report the detection of HCN J=4–3 and CS J=7–6 emission from the disk around HD 142527. The emission of both molecules is azimutally asymmetric, peaks towards the southwest of the disk and is suppressed in those regions with strong continuum emission. We discard a line-of-sight projection of the inner rim of the outer disk as origin of this asymmetry. We suggest two possible mechanisms that can drive this asymmetry related to the presence of a dust trap: [1] The flatter dust size distribution which drives a lower dust temperature. This in turn can lower the gas temperature and thus emissivity, and promote freeze out of CS and HCN molecules. [2] A higher (possibly optically thick in sub-mm wavelengths) continuum optical depth associated with increased dust concentrations which quenches line emission.

We thank the anonymous referee for the suggestions which helped make this manuscript more clear and concise, and

Michiel Min for sharing his model of HD 142527. GvdP, SC, SP, FM and VC acknowledge support from the Millennium Science Initiative (Chilean Ministry of Economy), through grant "Nucleus P10-022-F. GVDP, SP and SC acknowledge financial support provided by FONDECYT following grants 3140393, 3140601 and 1130949. WFT + FM acknowledge funding from the EU FP7-2011 under Grant Agreement nr. 284405. We further acknowledge funding from the European Commission's 7th Framework Program (contract PERG06-GA-2009-256513) and from the Agence Nationale pour la Recherche (ANR) of France under contract ANR-2010-JCJC-0504-01. This paper makes use of the following ALMA data: ADS/JAO.ALMA#2011.0.00465.S. ALMA is a partnership of ESO, NSF, NINS, NRC, NSC, and ASIAA. The Joint ALMA observatory is operated by ESO,AUI/ NRAO, and NAOJ.

Facilities: ALMA

REFERENCES

Acke, B., & van den Ancker, M. E. 2004, A&A, 426, 151
Avenhaus, H., Quanz, S. P., Schmid, H. M., et al. 2014, ApJ, 781, 87
Birnstiel, T., Dullemond, C. P., & Pinilla, P. 2013, A&A, 550, L8
Brown, J. M., Blake, G. A., Qi, C., et al. 2009, ApJ, 704, 496
Canovas, H., Ménard, F., Hales, A., et al. 2013, A&A, 556, A123
Casassus, S., Perez M., S., Jordán, A., et al. 2012, ApJ, 754, L31
Casassus, S., Hales, A., de Gregorio, I., et al. 2013, A&A, 553, A64
Casassus, S., van der Plas, G., M, S. P., et al. 2013, Nature, 493, 191
Christiaens, V., Casassus, S., Perez, S., van der Plas, G., & Ménard, F. 2014, ApJ, 785, L12
Dutrey, A., Guilloteau, S., & Guelin, M. 1997, A&A, 317, L55
Dutrey, A., Wakelam, V., Boehler, Y., et al. 2011, A&A, 535, A104
Fujiwara, H., Honda, M., Kataza, H., et al. 2006, ApJ, 644, L133
Fuente, A., Cernicharo, J., Agúndez, M., et al. 2010, A&A, 524, A19
Fukagawa, M., Tamura, M., Itoh, Y., et al. 2006, ApJ, 636, L153
Fukagawa, M., Tsukagoshi, T., Momose, M., et al. 2013, PASJ, 65, L14
Garrod, R. T., & Herbst, E. 2006, A&A, 457, 927
Guilloteau, S., Dutrey, A., Wakelam, V., et al. 2012, A&A, 548, A70
Högbom, J. A. 1974, A&AS, 15, 417
Honda, M., Inoue, A. K., Fukagawa, M., et al. 2009, ApJ, 690, L110
Kamp, I., Tilling, I., Woitke, P., Thi, W.-F., & Hogerheijde, M. 2010, A&A, 510, A18
Kastner, J. H., Zuckerman, B., Hily-Blant, P., & Forveille, T. 2008, A&A, 492, 469
Lyra, W., & Lin, M.-K. 2013, ApJ, 775, 17
Malfait, K., Waelkens, C., Bouwman, J., de Koter, A., & Waters, L. B. F. M. 1999, A&A, 345, 181
Miyake, K., & Nakagawa, Y. 1993, icarus, 106, 20
Öberg, K. I., Qi, C., Fogel, J. K. J., et al. 2010, ApJ, 720, 480
Öberg, K. I., Qi, C., Fogel, J. K. J., et al. 2011, ApJ, 734, 98
Perez, S., Casassus, S., Ménard, F. et al. submitted to ApJ
Pérez, L. M., Isella, A., Carpenter, J. M., & Chandler, C. J. 2014, ApJ, 783, L13
Pinte, C., Ménard, F., Duchêne, G., & Bastien, P. 2006, A&A, 459, 797
Pinte, C., Harries, T. J., Min, M., et al. 2009, A&A, 498, 967
Rameau, J., Chauvin, G., Lagrange, A.-M., et al. 2012, A&A, 546, A24
Semenov, D., & Wiebe, D. 2011, ApJS, 196, 25
Thi, W.-F., van Zadelhoff, G.-J., & van Dishoeck, E. F. 2004, A&A, 425, 955
van Boekel, R., Min, M., Leinert, C., et al. 2004, Nature, 432, 479
van der Marel, N., van Dishoeck, E. F., Bruderer, S., et al. 2013, Science, 340, 1199
van der Plas, G. 2010, Ph.D. Thesis, Chapter 6.
Verhoeff, A. P., Min, M., Pantin, E., et al. 2011, A&A, 528, A91
Walsh, C., Millar, T. J., & Nomura, H. 2010, ApJ, 722, 1607
Woitke, P., Kamp, I., & Thi, W.-F. 2009, A&A, 501, 383